Bioactive Materials 6 (2021) 2829–2840

Contents lists available at ScienceDirect

Bioactive Materials

journal homepage: www.sciencedirect.com/journal/bioactive-materials

A mussel-inspired supramolecular hydrogel with robust tissue anchor for rapid hemostasis of arterial and visceral bleedings

Ziwen Qiao [a,1], Xueli Lv [c,1], Shaohua He [d,1], Shumeng Bai [c], Xiaochen Liu [b], Linxi Hou [a], Jingjing He [a], Dongmei Tong [b], Renjie Ruan [a], Jin Zhang [a,*], Jianxun Ding [e,**], Huanghao Yang [b,***]

[a] Qingyuan Innovation Laboratory, College of Chemical Engineering, Fuzhou University, 2 Xueyuan Road, Fuzhou, 350108, PR China
[b] MOE Key Laboratory for Analytical Science of Food Safety and Biology, State Key Laboratory of Photocatalysis on Energy and Environment, College of Chemistry, Fuzhou University, 2 Xueyuan Road, Fuzhou, 350108, PR China
[c] College of Biological Science and Engineering, Fuzhou University, 2 Xueyuan Road, Fuzhou, 350108, PR China
[d] Department of Pediatric Surgery, Fujian Provincial Hospital, 134 Dongjie Road, Fuzhou, 350001, PR China
[e] Key Laboratory of Polymer Ecomaterials, Changchun Institute of Applied Chemistry, Chinese Academy of Sciences, 5625 Renmin Street, Changchun, 130022, PR China

ARTICLE INFO

Keywords:
Mussel-inspired hydrogel
Supramolecular cross-linking
Robust tissue anchor
Hemostatic sealant
Arterial and visceral bleeding models

ABSTRACT

In recent years, the developed hemostatic technologies are still difficult to be applied to the hemostasis of massive arterial and visceral hemorrhage, owing to their weak hemostatic function, inferior wet tissue adhesion, and low mechanical properties. Herein, a mussel-inspired supramolecular interaction-cross-linked hydrogel with robust mechanical property (308.47 ± 29.20 kPa) and excellent hemostatic efficiency (96.5% ± 2.1%) was constructed as a hemostatic sealant. Typically, we combined chitosan (CS) with silk fibroin (SF) by cross-linking them through tannic acid (TA) to maintain the structural stability of the hydrogel, especially for wet tissue adhesion ability (shear adhesive strength = 29.66 ± 0.36 kPa). Compared with other materials reported previously, the obtained CS/TA/SF hydrogel yielded a lower amount of blood loss and shorter time to hemostasis in various arterial and visceral bleeding models, which could be ascribed to the synergistic effect of wound closure under wet state as well as intrinsic hemostatic activity of CS. As a superior hemostatic sealant, the unique hydrogel proposed in this work can be exploited to offer significant advantages in the acute wound and massive hemorrhage with the restrictive access of therapeutic moieties.

1. Introduction

Massive hemorrhage originated from vital organ wounds always causes severe health hazards, especially for aortic and viscera rupture [1]. If without prompt treatment and hemostasis after injuries, excessive blood loss and even death might occur. Thus, a fast and effective wound hemostatic sealant for treating hemorrhage tissues caused by trauma is urgently needed. Currently, many commercial hemostats have been developed for realizing rapid hemostasis, such as Curspon®, zeolite-based QuickClot®, Surgicel®, and fibrin-based bandages [2–4]. They have been demonstrated to be highly effective in terminating bleeding but are often invalid for deep wounds because of irregular shape and low elasticity. Moreover, these materials are scarcely applicable to arterial and viscera wounds, owing to their weak wet tissue surface adhesion, poor hemostatic function, and insufficient mechanical performance [5].

Except for the commercial hemostat agents aforesaid, a hybrid hydrogel system with multiple coordinated mechanisms has also been proved to be a promising candidate for rapid hemostasis. Specifically, some hemostatic materials with the capacity of absorbing water from the blood, concentrating blood components at the hemorrhagic site [6], activating blood coagulation cascade, and/or providing a physical

Peer review under responsibility of KeAi Communications Co., Ltd.
* Corresponding author.
** Corresponding author.
*** Corresponding author.
E-mail addresses: J_Zhang929@fzu.edu.cn (J. Zhang), jxding@ciac.ac.cn (J. Ding), hhyang@fzu.edu.cn (H. Yang).
[1] Z. Qiao, X. Lv, and S. He contributed equally to this work.

https://doi.org/10.1016/j.bioactmat.2021.01.039
Received 30 October 2020; Received in revised form 18 January 2021; Accepted 30 January 2021

barrier to blood flow have been developed recently [7]. For example, Bu *et al.* reported a tetra-PEG-based hydrogel sealant with an excellent hemostatic function even under the anticoagulated conditions, displaying favorable biocompatibility and feasibility [8]. A unique double-network hydrogel was successfully prepared as a commercially-available hemostatic dressing by introducing two different chitosan (CS) chains *via* the simultaneous cross-linking of carbon–carbon double bonds and catechol-Fe^{3+} chelation [9]. However, the limited hemostatic efficiencies of these systems are only ideal for stopping vein hemorrhage or a small amount of bleeding, being far away from meeting the requirements of clinical applications for massive arterial bleeding [10].

For achieving rapid hemostasis of arterial and visceral wounds, a robust wet tissue adhesion ability to close the wound in the presence of continuous blood flow is another critical factor to be considered. Mussel-inspired materials, such as poly(γ-glutamic acid)–dopamine (γ-PGA–DA) hydrogel with multiple foot proteins, have been applied as wound sealant by rapidly sealing a hemorrhaging wound and preventing the bleeding [11]. Similarly, tannic acid (TA), as one of the natural biomolecule-based adhesives, is capable of forming a reversible and robust interaction with wet tissue [12]. Specifically, the phenolic moieties of TA molecule has a high binding affinity to proteins in tissue biomolecules, which is also beneficial to improve the biological compatibility as confirmed by spatial conformation and molecular dynamics simulations [13]. CS has good hemostasis properties by accelerating and strengthening blood clots, and its protection against a wide range of bacteria further enhances its appeal as an active component in several commercial wound dressings [14]. Silk fibroin (SF) has attracted significant attention recently, owing to its mechanical property, air permeability, and abundant source. Simultaneously, the slow gelation rates and shortage of bioactive cues are major limitations for their biomedical applications [15]. Considering that wound closure is significant for fast hemostasis, the promoted erythrocyte aggregation of CS cations is envisioned to be combined with the superior wound closure ability of underwater hydrogel sealants. In specific, we intend to assemble CS with SF by cross-linking them through TA to maintain the structural stability of the hemostatic hydrogel.

Herein, we proposed a strategy for achieving visceral hemostasis by designing a hydrogel sealant that simultaneously afforded a quick blood absorption, a robust wet adhesion, and wound closure capability. As shown in Scheme 1A, an injectable hemostatic CS/TA/SF hydrogel with supramolecular physical cross-linking-network structure was prepared and applied in various large dose hemorrhage models of rats and rabbits. Both amino/hydroxyl groups in CS branch chains and amide groups in SF form hydrogen bonds with phenolic hydroxyl groups in TA, based on the cross-linked CS/SF network (Scheme 1B). Supramolecular materials assembled from two or more molecular entities *via* non-covalent binding interactions demonstrated unprecedented advantages in biological applications because of the strong molecular interactions and the capability to incorporate various therapeutic agents [16]. The proposed hydrogel exhibited an ideal coagulation capacity of erythrocytes dependent on a rapid blood absorption speed, an excellent

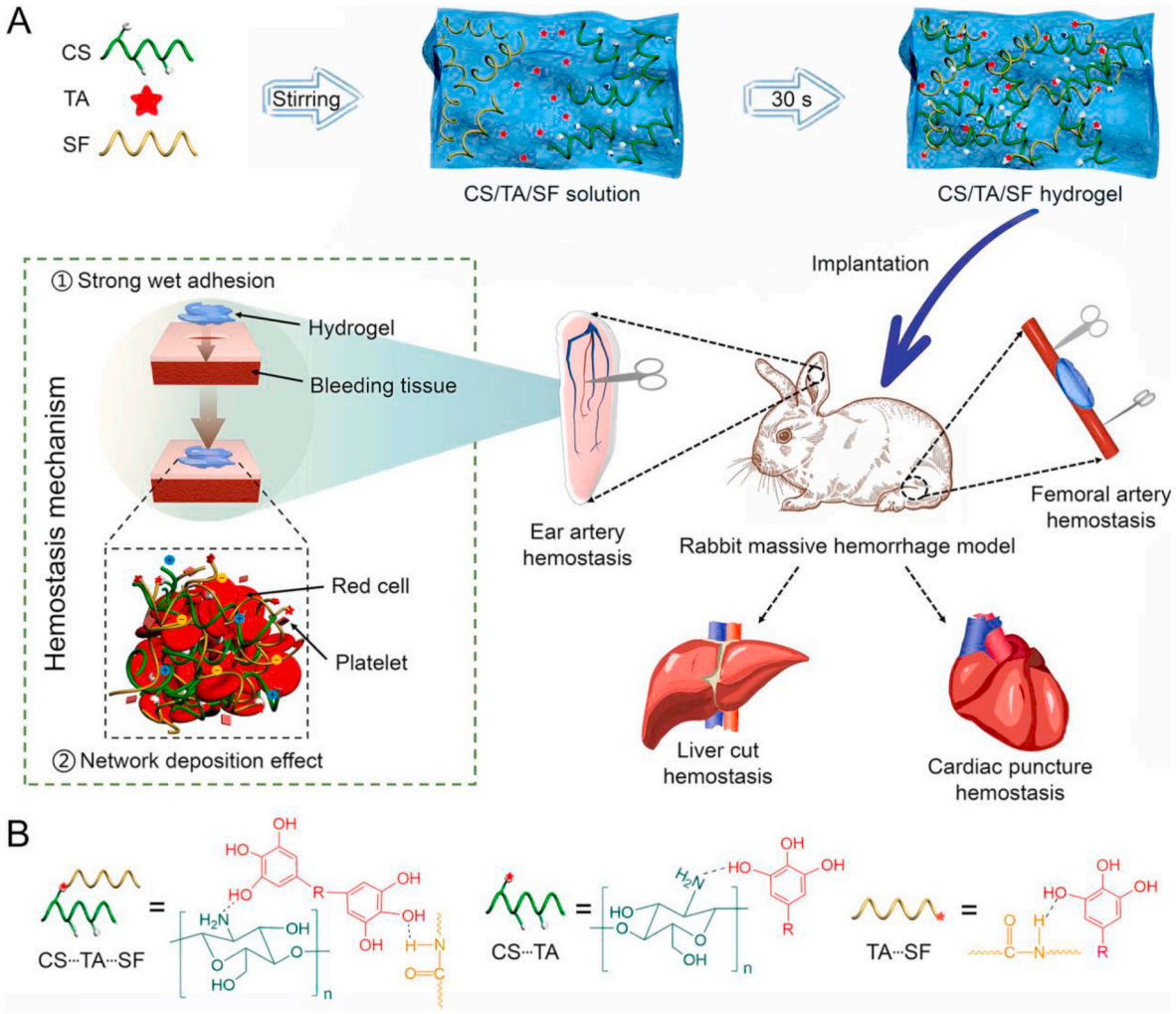

Scheme 1. Schematic illustration of (A) preparation and (B) cross-linking-network structure of CS/TA/SF hydrogel for massive arterial and visceral hemorrhage.

blood-clotting ability, and a high erythrocyte adhesion of CS. A robust wet adhesion property with a shear adhesion strength of 29.66 ± 0.36 kPa was verified, further benefiting from improving the hemostatic efficiency up to the highest value of 96.5% ± 2.1% reported so far. More interestingly, our viscous CS/TA/SF hydrogel presented faster blood clotting and wound closure *in vivo* than the gauze and no-treatment groups, owing to the desirable hemostatic function and tissue defect closure ability. On the whole, the mussel-inspired supramolecular physical cross-linking-network hydrogel with robust tissue anchor and rapid blood clotting offers significant advantages in the acute wound and massive hemorrhage with the restrictive access of therapeutic moieties.

2. Material and methods

2.1. Materials

Bombyx mori cocoons were purchased from Guangxi Tianyou Silk Co., Ltd. (Nanning, P. R. China). TA was obtained from Sigma-Aldrich Co., Ltd. (St. Louis, MO, USA). CS was purchased from Beijing Macklin Co., Ltd. (Beijing, P. R. China). All chemicals were received and used without further purification.

2.2. Synthesis of CS/TA/SF hydrogel

SF aqueous solution was first prepared according to our previous work [17]. Briefly, 10.0 g of Bombyx mori cocoon was boiled in 4.0 L of 0.02 M sodium carbonate (Na_2CO_3) solution for 20 min to remove the sericin protein. 13.5 g of the degummed cocoon was dissolved in 50.0 mL of 9.3 M lithium bromide (LiBr) solution for 3 h and then dialyzed for 72 h to get the 5.0 wt% SF solution. Second, 3.0 g of TA was dissolved in 10.0 mL of distilled water to obtain the solution with a concentration of 0.3 g mL^{-1}. In the meantime, 9.0 g of CS was dissolved in an aluminium trichloride ($AlCl_3$) solvent at 37 °C to harvest 30 wt% CS solution. Finally, the obtained TA and CS solutions were added to SF in different weight ratios, and the adhesive CS/TA/SF hydrogel was instantly formed after mixing these three solutions.

2.3. Adhesion testing

Tissue adhesive strength of the hydrogel was assessed by lap shear test on an Instron machine 1185 (Instron, Boston, MA, USA), using a 100 N load cell with the ASTM standard (F2255-05 method) [18]. Especially, fresh porcine skin purchased from a local supermarket was cut into slices with a size of 3.0 cm × 1.0 cm and 3.0 mm in thickness. CS/TA/SF hydrogel was mixed directly on the surface of porcine skin and cut into a size of approximately 1.0 cm × 1.0 cm. Subsequently, two porcine skin tissues covered by the hydrogel were contacted closely with opposite direction overlaps. After keeping the samples in a damp chamber for 20 min, they were placed in the machine to test the shear strength. All the experimental data were repeated thrice.

2.4. Blood clotting index

The blood clotting index (BCI) was performed according to the method modified by Shih *et al.* [19]. First, CS/TA/SF hydrogel was cut into a 1.0 × 1.0 × 0.2 cm^3 cube, placed into the polypropylene dish, and pre-warmed at 37 °C for 5 min. Second, blood taken from the rat heart was clotted by adding 0.1 M calcium chloride ($CaCl_2$) solution (10:1), and 200.0 μL of the clotted blood was coated onto the dressing immediately. Third, after incubating the samples at 37 °C for 60 min, 5.0 mL of deionized water was added to the dish and shaken at 50 rpm for 10 min to lyse red blood cells (RBCs) that were not stuck in the clot. The absorbance of the resulting hemoglobin solution (sample) was measured at 540 nm by a Jasco V-630 spectrophotometer (Jasco Company, Ishikawamachi, Tokyo, JPN), and absorbance of 200.0 μL of clotted whole blood in 5.0 mL of deionized water was used as a reference. Finally, the BCI of CS/TA/SF hydrogel was calculated using the following Equation (1):

$$\mathrm{BCI} = \frac{A_{\mathrm{sample}}}{A_{\mathrm{control}}} \times 100\% \quad (1)$$

2.5. Blood fluid uptake property

Heparinized mouse blood was used to test the blood fluid uptake property of CS/TA/SF hydrogel. 300.0 μL of heparinized mouse blood was mixed with the same amount of CS/TA/SF hydrogel in 1.5 mL of the centrifuge tube, which was then kept at 37 °C, and time was recorded immediately. The inverted tube test was used to determine whether the blood was clotted completely. Finally, the clotting time was averaged in three replicates, and the blank control was treated without a sample.

2.6. Erythrocyte adhesion

Adhesive microstructures of RBCs to CS/TA/SF hydrogel were characterized by scanning electron microscopy (SEM; FEI Company, Hillsboro, OR, USA). Before the experiment, fresh blood taken from the rat heart with a medical vacuum collective tube containing heparin anticoagulant was centrifuged at 3,000 rpm for 15 min at room temperature, and the supernatant was then discarded to obtain the erythrocytes. The RBCs were washed with phosphate-buffered saline (PBS) thrice and diluted into 10% of the initial concentration. CS/TA/SF hydrogel was cut into 0.5 × 0.5 × 0.5 cm^3 cube, which was placed into a polypropylene dish and prewarmed for 5 min at 37 °C, and then 200.0 μL of diluent was dispensed onto the dressing. After incubating at 37 °C for 0.5 h, the dressing was rinsed twice with PBS to remove non-adhered erythrocytes. The adhered erythrocytes were stabilized with 2.5% (*V/V*) glutaraldehyde for 0.5 h and then gradually dehydrated with 70%, 80%, 90%, and 100% (*V/V*) ethanol for 15 min. For the observation, all the samples were fixed onto the metal stub with double-sided adhesive copper tape, and a layer of AuPd film in 10.0 nm thickness was sprayed under vacuum. The sample was imaged using SEM at an accelerated voltage of 3 kV.

2.7. Animal hemostasis experiments for rats

The hemostatic ability of CS/TA/SF hydrogel was estimated on a male Sprague-Dawley rat (200.0–250.0 g), which was narcotized and fixed as described above. For tail hemostasis of rat, a third of the tail was cut by surgical scissors and then exposed to air for 15 s to allow an average blood loss. Afterward, the wound was covered with 300.0 μL of the hydrogel, commercial gauze, or without treatment. For liver hemostasis of rat, the chest of the rat was opened, and a cut of 2.0 cm × 0.5 cm was created on the liver. Free bleeding was allowed for 20 s, and then 1.2 mL of CS/TA/SF hydrogel was immediately injected into the defect. In terms of *in vivo* hemostasis on the heart of rat, the chest was dissected to expose the heart, and the bleeding was induced using an 18-gauge needle. After bleeding for 5 s, 800.0 μL of the hydrogel was put onto the bleeding point of the beating heart. Groups without any treatment and treated with gauze were used as controls. Once the hemostasis was achieved, the clotting time (s) and blood loss were recorded immediately.

2.8. Animal hemostasis experiments for rabbits

New Zealand White rabbit (male, 2.5–3.0 kg) was used as a hemostasis model to evaluate the hemostatic capacity of CS/TA/SF hydrogel. All the rabbits were fixed onto a wooden corkboard for operation and were anesthetized with 3% (*W/V*) sodium pentobarbital by intravenous injection into the ear (0.3 mL per 100.0 g). For liver hemostasis of the rabbit, the rabbit underwent an abdominal incision to expose the liver,

and then a liver defect with a length of 3.0 cm and a depth of 5.0 mm was made using surgical scissors. Free bleeding was allowed for 20 s, and then 1.5 mL of CS/TA/SF hydrogel was immediately injected into the defect. The subsequent operation followed the method of hemostasis on the liver of rat. After being observed for 2 h, the rabbit was finally euthanized with an overdose of sodium pentobarbital.

The heart was exposed by separating it from the chest, and the bleeding was induced using a 23-gauge needle. After bleeding for 5 s, CS/TA/SF hydrogel was immediately applied to the bleeding point of the beating heart. Meanwhile, heart rate and blood pressure were monitored. For ear artery hemostasis of rabbit, the hair on the rabbit ear was cut off to expose the ear artery. The ear vein was cut at 7.0 cm from the tip of the ear to allow free bleeding for 10 s. Subsequently, 600.0 μL of CS/TA/SF hydrogel was covered onto the hemorrhagic spot. With regard to the femoral artery hemostasis of rabbit, skin and soft tissues were peeled off by the surgical scalpel to show the femoral artery. The proximal and distal ends of the artery were clamped with hemostatic forceps and then incised by bistoury. The nip at both sides was released to allow a free bleeding loss for 10 s, subsequently applying 1.5 mL of CS/TA/SF hydrogel onto the hemorrhagic site.

All the animal experiments were executed according to the protocols approved by the Institutional Animal Care and Use Committee of Fuzhou University, and the experimental procedures were in agreement with the guide for the care and use of laboratory animals (Ministry of Science and Technology of China, 2006). Each hemostasis group contained at least three animals.

2.9. Statistical analysis

All data were expressed as mean ± standard deviation (SD). Statistical software of SPSS 13.0 was used to analyze the data by one-way analysis of variance (ANOVA). $^{*}P < 0.05$, $^{**}P < 0.01$, and $^{***}P < 0.001$ were defined as significant for all statistical tests.

3. Results and discussion

3.1. Comprehensive performance evaluation of CS/TA/SF hydrogels with different component proportions

To investigate the optimum composition of the hydrogel, the orthogonal experimental design was used to select a subset of combinations for experimentation, rather than all the combinations. Herein, a Taguchi L9 orthogonal array was employed to determine the formula of hemostatic hydrogel with anticipated comprehensive performance (Tables S1–S3, Supplementary data). Notably, the solid contents of hydrogels in different groups were maintained consistently by preparing

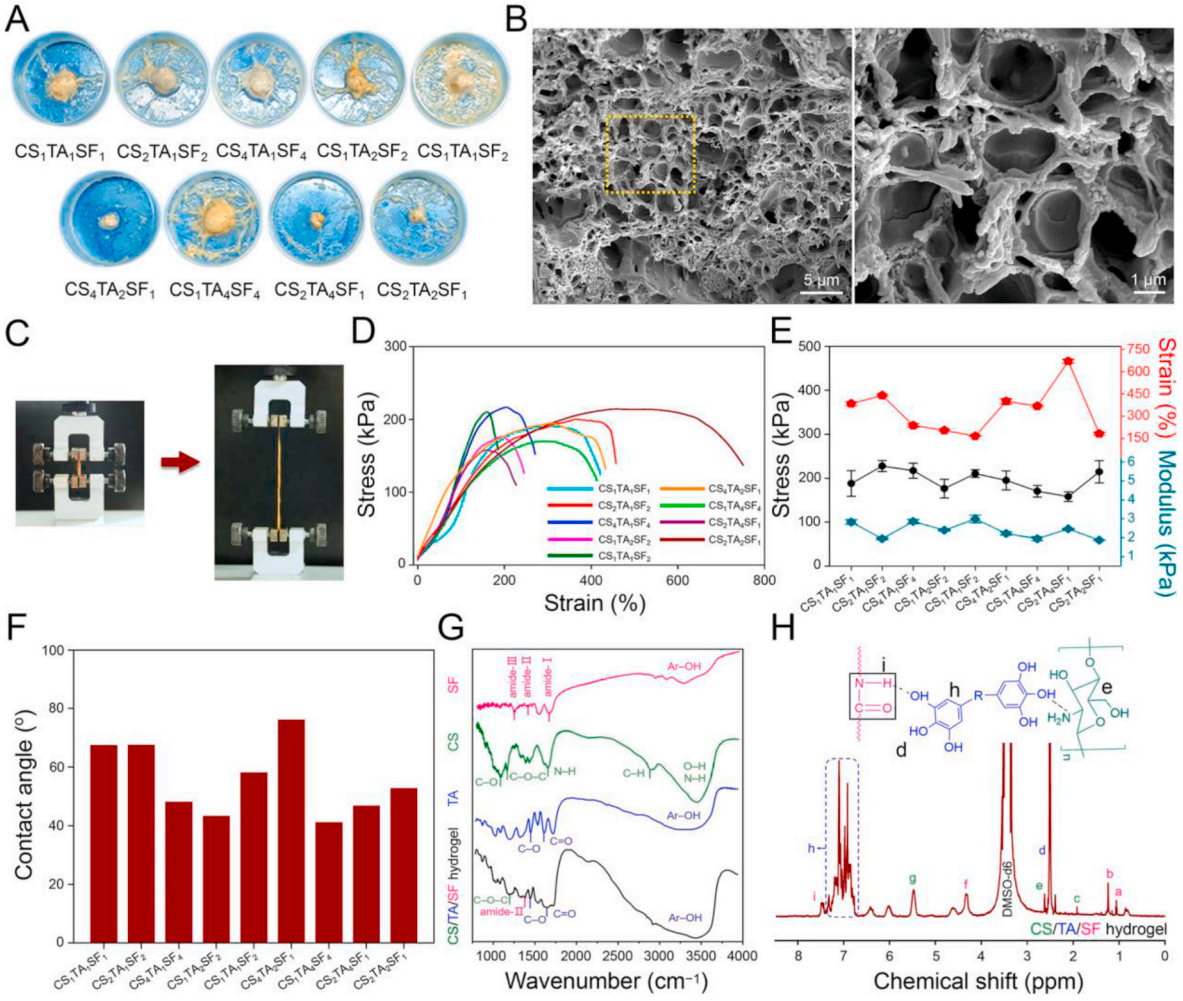

Fig. 1. Structural and physical properties of CS/TA/SF hydrogels with different weight ratios. (A) Photographs showing gross morphologies of hydrogels onto polypropylene dish. (B) SEM images of hydrogel after lyophilization. Right is the higher magnification image of the retangular area in the left one. (C) Tensile testing photograph of hydrogel. (D) Representative tensile stress–strain curves. (E) Comparison of tensile strength, strain, and Young's modulus of hydrogels with different weight ratios. (F) Contact angles for water droplet on hydrogel surface. (G) Conformational analysis of hydrogel by FTIR spectroscopy. (H) ^{1}H NMR spectra of hydrogel. All statistical data are represented as mean ± SD ($n = 3$; $^{***}P < 0.001$).

samples with the same total volume of 5.0 mL (Table S3, Supplementary data).

Fig. 1A shows the gross morphologies of hydrogels with different weight ratios selected from the orthogonal array. As observed, the formation of plenty of filaments was mainly caused by the attachment of phenolic hydroxyl groups onto the polypropylene dish, well mimicking the chemical composition of mussel foot proteins [20]. The phenolic moieties linked to the backbone of polymers also exhibited robust underwater adhesion performance [21]. $CS_4/TA_1/SF_4$ and $CS_1/TA_4/SF_4$ hydrogels achieved the highest production rates and the most intact morphologies, which formed the hydrogels with abundant feet to glue onto the dish. This phenomenon was attributed to the affinity of SF during the co-assembly process, while too much positive charge on the surface of CS affected hydrogel formulation in low productive rate group.

Furthermore, porous morphology and surface roughness of CS/TA/SF hydrogel were observed by SEM (Fig. 1B). Pores with diameters located in the range of 0.5–2.5 μm were homogeneously distributed in the hydrogel matrix. In the meantime, the supramolecular physical cross-linking-network structure and a certain degree of roughness of the pore wall were conducive to the adhesion and aggregation of RBCs. However, it was worth noting that pore sizes derived from SEM images revealed the value of CS/TA/SF hydrogel under a dry state. There were likely orders of magnitudes in difference instead of directly comparable.

Generally, hydrogels prepared by natural materials presented weak mechanical strength, which might hinder their applications for hemostasis and wound closure. However, incorporating CS, TA, and SF into a network significantly reinforced the mechanical property of the hydrogel [22]. As illustrated in Fig. 1C–E, the hydrogel showed high mechanical strength (158.54 ± 10.90 kPa–227.87 ± 12.60 kPa), which was ascribed to the excellent ductility of CS/SF and the existence of an interpenetrating polymer cross-linking network. Young's moduli of hydrogels in all groups were higher than 91.37 ± 1.43 kPa, and $CS_1/TA_1/SF_2$ hydrogel even reached up to 197.97 ± 3.50 kPa, being approximated to the moduli of living tissues.

Adequate water absorption capacity was also crucial for medical hemostatic materials. It was hypothesized that the high absorptive capacity of wound dressing would lead to the aggregation of erythrocytes, platelets, and other blood coagulation factors onto the surface of materials, and finally resulted in the formation of blood clotting as well as the enhanced hemostasis ability [23]. The hydrophilicity and surface absorption ability of the prepared hydrogels were evaluated by water contact angles (WCAs). As observed from Fig. 1F, contact angles of all the hydrogels were lower than 90°. More interestingly, these water droplets were soaked up and disappeared swiftly on the surface of a hydrogel in seconds (Movie S1, Supplementary data), similar to the strong water absorption behavior of sponge [24,25]. Such superior hydrophilicity and hygroscopicity were ascribed to the following two factors. CS is a hydrophilic polymer, which has many hydroxyl (−OH) and amino ($-NH_2$) groups, and TA with phenolic hydroxyl groups is also highly hydrophilic and shows good solubility in water [26]. On the other hand, a stable porous structure of the hydrogel with a high cross-linking degree is beneficial for commencing gas (O_2 and CO_2) exchange [27], absorbing exudate from an injury surface, and inhibiting exudate accumulation from minimizing detrimental effect at the wound site [28]. Overall, such supramolecular cross-linking hydrogel can effectively absorb water in serum to concentrate coagulation factors and red blood cells, thereby preventing blood from flowing out and achieving rapid hemostasis [29].

Supplementary video related to this article can be found at https://doi.org/10.1016/j.bioactmat.2021.01.039

Fourier transform infrared spectroscopy (FTIR) spectroscopy verified the structural formation of CS/TA/SF hydrogel (Fig. 1G). The band presented at 1508 cm^{-1} belonged to the stretching and bending modes of amide II (C–H and N–H) bonds in SF, and C–H at 2980 cm^{-1} as well as C–O–C bonds at 1150 cm^{-1} were detected in CS. The absorption bands caused by stretching of C–O bond at 1544 cm^{-1} and stretching of C═O bond at 1666 cm^{-1} were also observed in the spectrum of TA [30]. A slight shift of phenolic hydroxyl (Ar–OH) group to the left was attributed to the formation of a hydrogen bond with the amide II group after gelation. While, wide absorption band appeared at 3,000−3,600 cm^{-1} meant that the Ar–OH group was well preserved after a chemical reaction, which provided a robust wet adhesion of the hydrogel. Characteristic functional groups described above were all detected in such unique complex hydrogel, suggesting that the reactants aforementioned were all successfully introduced to form new substances.

A representative proton nuclear magnetic resonance spectroscopy (^1H NMR) spectrum of the self-assembled CS/TA/SF hydrogel was depicted in Fig. 1H. The peaks of CH–CH–CH–CH_2 groups at "*e*" (2.62 ppm) were ascribed to the *N*-acetylglucosamine ring protons from CS [31]. Alanine β-CH_2 at "*b*" (1.23 ppm) and amide II groups in SF observed at "*i*" (7.48 ppm) were used as a reference to demonstrate the conjugation of TA and SF [32]. After the reaction of CS, TA, and SF, phenolic hydroxyl proton peaks at 2.50 ppm and deprotonation peaks at "*h*" (6.76–7.32 ppm) appeared in the meantime [33].

Ideal hemostatic material should promote quick coagulation to minimize blood loss. The hemostatic ability of CS/TA/SF hydrogel was investigated in an *in vitro* clot formation model, where the whole blood was dropped onto the hydrogel and polypropylene dish for 2 min to compare their blood pro-coagulant efficacy (Fig. 2A). The speed of blood clotting for $CS_2/TA_4/SF_1$ hydrogel was much higher than that in the untreated situation during the same test period, and the blood discoloration was visibly deeper for the hydrogel. These results indicated that the proposed composite hydrogel quickly absorbed blood and accumulated RBCs and platelets on the material surface, promoting blood coagulation.

The hemostatic mechanism of such CS/TA/SF hydrogel was shown in Fig. 2B. Water-soluble TA contained many hydrophilic polyphenols that were consisted of five catechols and gallols at termini [34], and it underwent self-assembly aggregation *via* hydrogen bonding. In addition, TA was an ideal gelation binder for hydrogel formation [35]. The polyphenol groups of TA had a high binding affinity with nucleophiles (*e.g.*, amido bond, amines, and thiol), and thus tightly bound to biological molecules, such as proteins and peptides [18,36]. Given the multi-aromatic ring structure, TA combined with amino acids in SF and amino groups in CS through electrostatic interactions and hydrogen bonds to maintain the structural stability of the hydrogel. Such a supramolecular-network structure was crucial in absorbing wound exudates and blocking the escape of RBCs and platelets as a hemostatic agent. CS owned an excellent hemostatic property because of its ability to form cationic clusters through interacting with anions on RBCs, thereby inducing platelet aggregation and eventually stopping blood loss [37]. Specifically, the bridging segment of CS was adsorbed on the cell surface by non-specific forces, including van der Waals force, electrostatic force, and hydrogen bond, promoting the change of hemorheology and completing coagulation of erythrocytes. As SF and TA accelerated blood clots *via* direct interaction with platelets and coagulation factors, the copolymerization of these three materials further exerted a positive synergistic effect on enhancing hemostasis [38].

To systematically investigate the effect of CS, TA, and SF content on blood clotting performance, CS/TA/SF hydrogels with various proportions were tested (Fig. 2C). 200.0 μL of the whole blood was slowly dispensed on the surface of different hydrogels, then incubated at 37 °C for 60 min. After adding distilled water to the blood clotting carefully, RBCs not entrapped in the clots were hemolyzed with water. Only $CS_1/TA_1/SF_1$, $CS_2/TA_1/SF_2$, $CS_4/TA_2/SF_1$, and $CS_2/TA_4/SF_1$ hydrogels showed a noticeable blood crust remaining on the hydrogels, and their corresponding hemostatic efficiencies reached up to high values of above 90% (Fig. 2D), indicating that hydrogels in these compositions had excellent blood clotting capacities and were especially desired in the field of hemostasis.

Simultaneously, a microplate reader was employed to test the

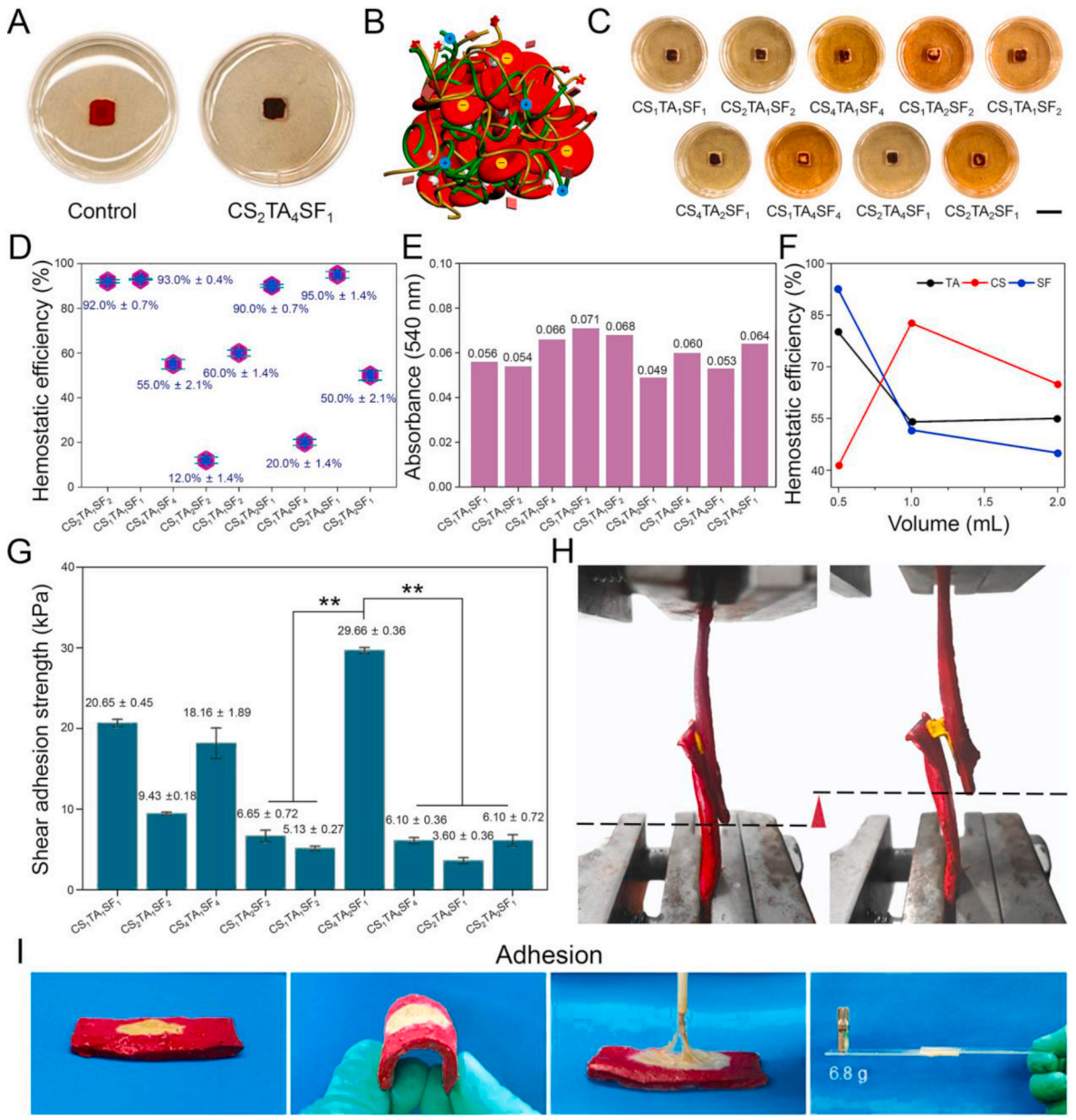

Fig. 2. Hemostatic performances and wet shear adhesion strengths of CS/TA/SF hydrogels with different weight ratios. (A) Photographs showing clot formation on hydrogel and polypropylene dish. (B) Schematic illustration of hemostatic mechanism. (C) Photographs showing blood pro-coagulant efficacies of hydrogels (scale bar = 10 mm). (D) Hemostatic efficiencies of hydrogels. (E) Absorbance of hemoglobin tested by microplate reader. (F) Changes of hemostatic efficiencies with different volume ratios of CS, TA, and SF. (G) Shear adhesion strength of hydrogel using wet porcine skin as substrate. (H) Lap shear testing photographs of hydrogel using an Instron machine 1185. (I) Photographs showing a strong adhesion of hydrogel with wet porcine skin and glass. All statistical data are represented as mean ± SD ($n = 3$; $^{*}P < 0.05$, $^{**}P < 0.01$, $^{***}P < 0.001$).

absorbance of resultant hemoglobin solution at 540 nm. In this measurement, the absorbance value was related to the concentration of free RBCs in the whole blood, so the clotting rate was negatively correlated with the absorbance value [39]. As can be seen from the column charts in Fig. 2E, $CS_1/TA_1/SF_1$, $CS_2/TA_1/SF_2$, $CS_4/TA_2/SF_1$, and $CS_2/TA_4/SF_1$ hydrogels showed lower absorbance values compared with other groups, complying with the hemostatic efficiency we obtained above. Fig. 2F shows the effects of three components on the hemostatic efficiency of CS/TA/SF hydrogel, according to which the hemolysis performance would be maximized by adjusting the composition ratio.

Current hemostatic materials are challenging to control hemorrhaging from the acute arterial and visceral wounds, owing to their weak adhesion on wet and flexible tissues. Hydrogel adhesive strength on wet tissue was another critical factor influencing the efficiency of wound closure and hemolysis, because the hydrogel acted as a hemostat or sealant allowed proper healing to occur by preventing blood leakage from the tissue [40]. Therefore, wet shear adhesion strengths of CS/TA/SF hydrogels with different weight ratios were also evaluated herein according to the ASTM standard method [41]. A lap shear test was used to identify the shear adhesive strength of the hydrogel on wet porcine skin, and the results were exhibited in Fig. 2G–H. An evident displacement could be observed before and after stretching CS/TA/SF hydrogel, and the maximum shear adhesive strength of 29.66 ± 0.36 kPa was achieved in $CS_4/TA_2/SF_1$ hydrogel. Movie S2 (Supplementary data) also demonstrated the strong adhesion ability of the hydrogel onto wet tissue like porcine skin. Such beneficial wet adhesion properties of the obtained hydrogels were derived from phenolic hydroxyl groups that tightly bonded with amino groups on tissue surface, and at the meantime

its internal supramolecular network also generated reliable mechanical strength. The robust adhesion allowed application of CS/TA/SF hydrogel in an effortless mode and promoted its clinical translation.

Supplementary video related to this article can be found at https://doi.org/10.1016/j.bioactmat.2021.01.039

Such superior adhesion performance can be intuitively demonstrated in another way. As shown in Fig. 2I, when the porcine skin was bent over 180°, CS/TA/SF hydrogel deformed with no shrink and remained to attach onto its surface. In addition, the hydrogel firmly adhered to the porcine skin when it was pulled with a stick. More interestingly, the hydrogel withstood a weight of 6.8 g at room temperature as two pieces of glasses adhered together by it. Because of its powerful coagulating effect through binding biomacromolecules, it was rational to believe that CS/TA/SF hydrogel could be employed as an effective hemostatic sealant to stop blood loss. The introduction of appropriate CS into the hydrogel maintained its capacity for wet wound sealing and enhanced hemostatic property, thus significantly increasing the clinical utility of the composite CS/TA/SF hydrogel as an efficient hemostat.

3.2. *In vitro hemostasis and biocompatibility of $CS_2/TA_1/SF_1$ hydrogel with optimized formulation*

According to the design rules of orthogonal experiments, $CS_2/TA_1/SF_1$ hydrogel was determined as the optimal group based on its high hemostatic efficiency and favorable comprehensive performance (Table S4, Supplementary data). First, the hydrogel showed excellent

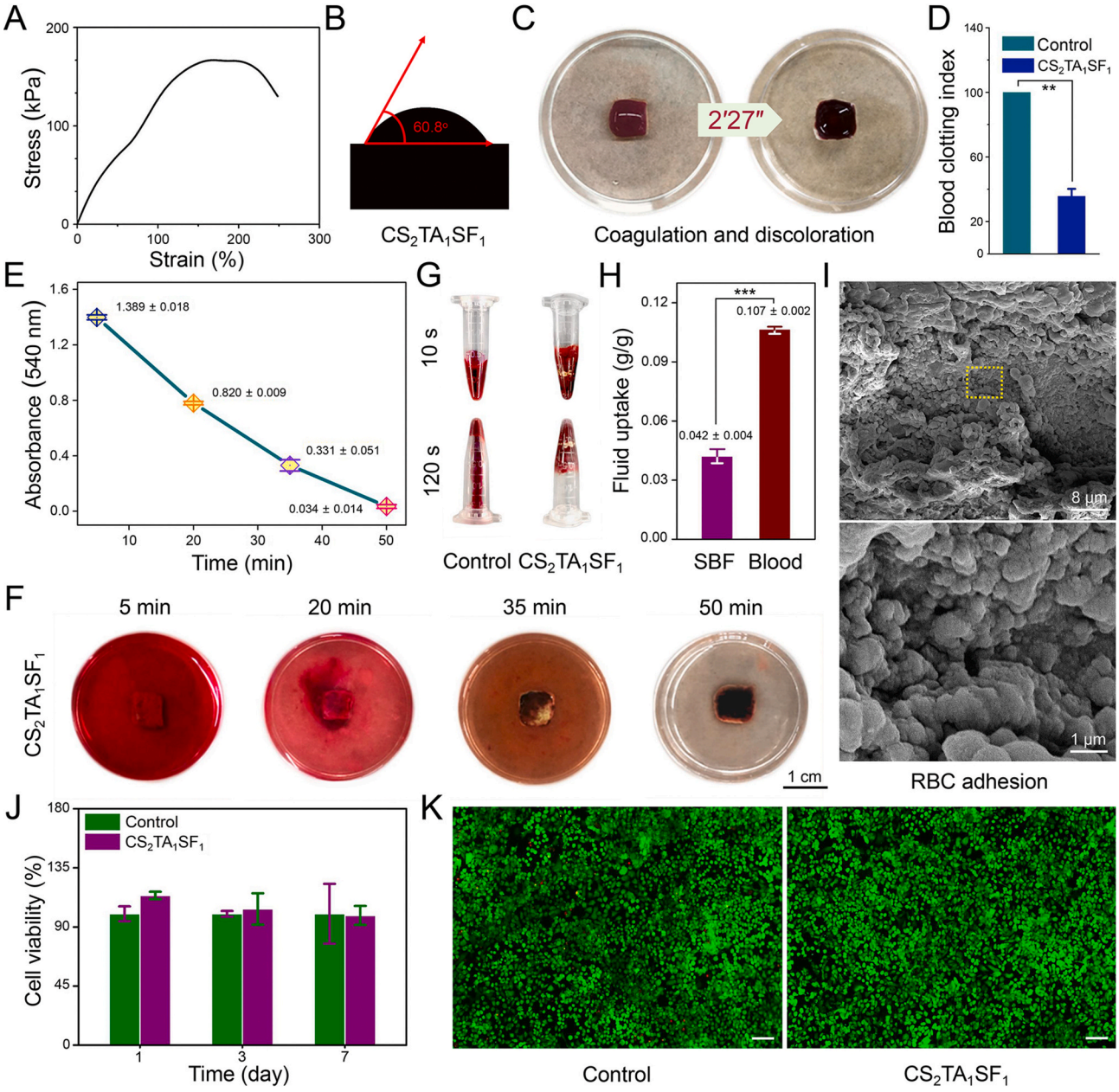

Fig. 3. Comprehensive performance of $CS_2/TA_1/SF_1$ hydrogel with optimized weight ratio. (A) Representative tensile stress–strain curve. (B) WCA measurement. (C) Blood clotting test and (D) BCI of control and sample groups. (E) Whole blood clotting kinetics of hydrogel. (F) Digital photographs of blood absorption kinetics test as a function of time. (G) Photographs of blood coagulation treated with CS/TA/SF hydrogel or nothing. (H) SBF and blood uptake ability of hydrogel. (I) SEM morphologies of RBC adhesion on hydrogel. Below is the higher magnification image of the retangular area in the above one. (J) CCK-8 assay result of LO2 cells. (K) Live-dead staining images of LO2 cells encapsulated in hydrogel after seven days of incubation (scale bar = 100 μm). All statistical data are represented as mean ± SD ($n = 3$; $^{***}P < 0.001$).

ductility with an elongation rate of 220.3% ± 9.2% and high tensile strength of 179.08 ± 0.30 kPa (Fig. 3A). The formation of supramolecular physical cross-linked-network enabled the hydrogel with good elasticity, which was beneficial for wound treatment application. WCAs were also explored to evaluate water absorption capacity. As shown in Fig. 3B, $CS_2/TA_1/SF_1$ hydrogel had a low contact angle of 61.0° ± 1.1° and retained a large amount of water to maintain a moist environment of the wound site. Such good hydrophilicity and water absorptiveness were conducive for the hydrogel to stop bleeding and promote wound healing quickly.

The optimized $CS_2/TA_1/SF_1$ hydrogel was also verified with good coagulation efficiency, where blood was completely coagulated and allochroic during a short time of 2′27″ (Fig. 3C). The blood clotting result of RBCs in the hemostatic hydrogel was shown in Fig. 3D. It can be seen that BCI of $CS_2/TA_1/SF_1$ hydrogel was higher than that of simulated body fluid (SBF), suggesting that the hydrogel quickly absorbed water from the blood, increased blood viscosity, and then promoted aggregations of RBCs and platelets.

Consistent with quantitative results, $CS_2/TA_1/SF_1$ hydrogel also exhibited a high blood absorption capacity. As shown in Fig. 3E–F, whole blood clotting kinetics of the hydrogel presented an increasing clotting rate as time went on (5–50 min), and the corresponding absorbance value of the blood was decreased from 1.389 ± 0.018 to 0.034 ± 0.014. Blood coagulation is a dynamic process, during which each coagulation element is performed effectively in a certain order and eventually converts fibrinogen to fibrin. In the present study, RBCs were aggregated by amine groups of CS and tangled by the supramolecular network structure. The hydrogel well mimicked the chemical compositions and hierarchical nanostructures of mussel foot proteins, which was more conducive to the aggregation and adhesion of erythrocytes.

A favorable coagulating function of $CS_2/TA_1/SF_1$ hydrogel was further demonstrated by mixing it with 1.0 mL of mouse blood for 10 s. Different from the control group, blood incubated with the hydrogel nub lost its flowability and held their weight upon tube inversion at 120 s later (Fig. 3G). Such short blood clotting time for $CS_2/TA_1/SF_1$ hydrogel was beneficial for an expeditious *in vivo* hemostasis. The presence of $CS_2/TA_1/SF_1$ hydrogel reduced the blood clotting time, which indicated an accelerated platelet aggregation and activated clotting factors caused by the strong interaction between phenolic moiety in the hydrogel and nucleophiles in blood proteins [42].

Absorption efficiency of $CS_2/TA_1/SF_1$ hydrogel was determined upon mouse blood and SBF, as shown in Fig. 3H. After immersing the hydrogel in respective fluids for 1 h, it was found that the material absorbed blood approximately two times as much as SBF (0.107 ± 0.002 g/g compared to 0.042 ± 0.004 g/g). The result demonstrated that our hydrogel had an excellent blood absorption ability to achieve rapid

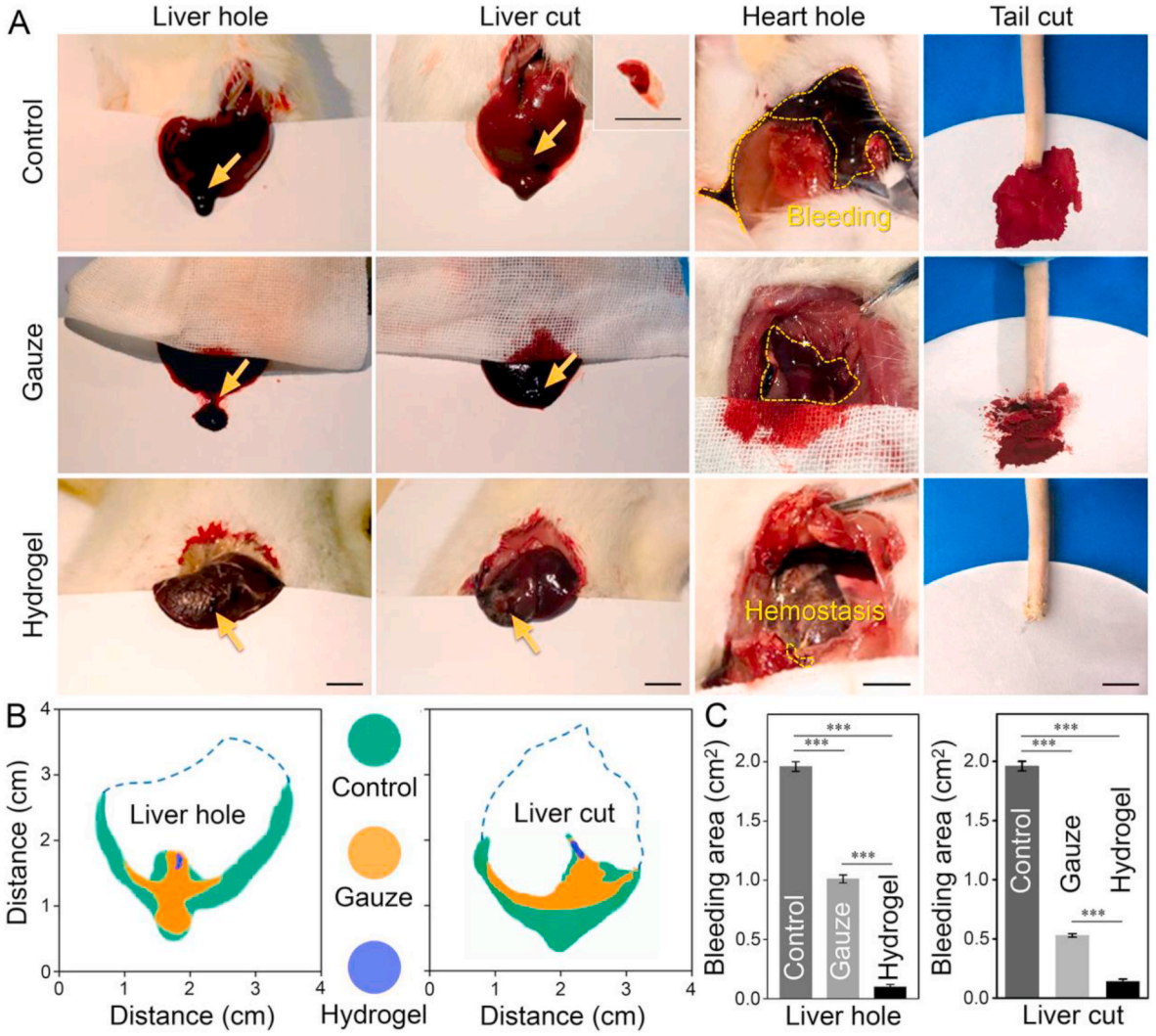

Fig. 4. Hemostatic property of $CS_2/TA_1/SF_1$ hydrogel in various damage models of rats. (A) Hemostatic images of covering gauze or hydrogel on various wounds with no treatment as a control (scale bar = 1 cm). (B) Comparison of bleeding area in the liver injury model. (C) Quantitative analysis of bleeding area for each group. All statistical data are represented as mean ± SD ($n = 3$; $^{***}P < 0.001$).

hemostasis. The adhesion capacity of RBCs is another critical indicator of hemostatic performance. The influence of hydrogel structure on the RBCs adhesion was observed by SEM (Fig. 3I). The cross-linked network structure and existence of CS in the composite hydrogel significantly enhanced the aggregation and adhesion of RBCs on the hydrogel surface.

Cell Counting Kit-8 (CCK-8) assay of LO2 cells was conducted to evaluate the cell viabilities quantitatively (Fig. 3J), and live−dead staining images of cells encapsulated in $CS_2/TA_1/SF_1$ hydrogel after seven days of incubation were shown in Fig. 3K. The cell viabilities treated with the hydrogel were comparable with those of the control group in 1, 3, and 7 days, indicating that majority of the cells survived well with low cytotoxicity on the hydrogel.

3.3. *In vivo hemostatic effect evaluation of $CS_2/TA_1/SF_1$ hydrogel*

To demonstrate the promising potential of $CS_2/TA_1/SF_1$ hydrogel as clinical hemostatic materials, they were employed for repairing a variety of acute tissue injuries, including liver, heart, and artery bleedings (Fig. 4A). First, the hemostatic property of $CS_2/TA_1/SF_1$ hydrogel was evaluated using a rat liver model, a specific visceral organ with abundant blood supply. It was observed that blood gushed from the pinholes as a quick pierce on the liver was conducted. The blood still flowed in such a liver puncture model if there was no treatment or covering with gauze. Differently, the hemorrhage site was quickly stopped bleeding in a few seconds with the presence of the hydrogel on pinhole. To further evaluate the hemostatic efficiency of proposed hydrogel, another liver bleeding model was created by knifing a thin sliver with a depth of 5.0 mm and a length of 30.0 mm. When the standard gauze was applied to the wound, there was no evident effect on hemostasis compared with no treatment group. However, the $CS_2/TA_1/SF_1$ hydrogel halted the blood loss immediately by swelling and forming a sealant, and complete hemostasis of the wound was visually observed.

Subsequently, an instant hemostatic capacity and a strict adhesion of the hydrogel were further demonstrated in a heart damage model, where the proposed sample tolerated a strong mechanical perturbation of heart beating that was filled with biofluids [43]. In detail, we created a lesion site with a needle from the heart to compare the clotting ability of various treatments. The bleeding could not be stopped by utilizing gauze even with the help of external pressure for 5 min, clearly proving that the blood clotting function of commercial gauze was minimal. On the contrary, such severe bleeding was successfully controlled once $CS_2/TA_1/SF_1$ hydrogel was covered on the wound, and no more bleeding came out 2 min later.

An amputating rat tail hemostatic model was used to further demonstrate that the hydrogel can achieve rapid hemostasis, as there was a large amount of blood gushing out from the injured site. When $CS_2/TA_1/SF_1$ hydrogel was placed on the wound, the blood loss was quickly stopped and presented an excellent hemostatic performance with almost no bloodstain left on the filter paper. Additionally, the composite hydrogel significantly facilitated hemostasis in less than 30 s, while the gauze needed at least 5 min to stop the bleeding, in line with our expectation about the outstanding hemostatic performance of the unique hydrogel. In summary, these results indicated that $CS_2/TA_1/SF_1$ hydrogel possessed an excellent *in vivo* hemostatic capability and was able to overcome the challenges of most arterial bleeding conditions.

The bleeding area in the liver injury model was measured to evaluate the hemostatic effect of $CS_2/TA_1/SF_1$ hydrogel quantitatively. As shown in Fig. 4B−C, applying the hydrogel onto the wound site decreased the bleeding area for both models compared with the untreated and gauze groups. Specifically, the presence of the hydrogel on the wound site decreased the bleeding area to 1/20 of that in the untreated group, as can be seen in the bar chart. The H&E staining results of incisions of the five organs demonstrated that $CS_2/TA_1/SF_1$ hydrogel served as hemostatic and wound closure materials had excellent therapeutic effect and biosafety (Fig. S1, Supplementary data).

Noticeably, the wound sealing was achieved without the secondary hemorrhage, confirming the efficacy of $CS_2/TA_1/SF_1$ hydrogel for stanching the hemorrhage tissues even under highly dynamic environments. Such predominant hemostasis ability was attributed to strong tissue adhesion and direct blood-gelling capacity of the hydrogel, ignoring deficiency of the body's coagulation mechanism [44]. In detail, as the hydrogel was placed onto the bleeding site, it first displayed the function of the physical barrier immediately. On the other hand, an optimal water uptake capacity of the hydrogel was also beneficial for concentrating the erythrocytes, platelets, and blood coagulation factors, thus leading to rapid hemostasis.

Uncontrolled hemorrhage has become a significant concern in the military and civilian trauma centers across the world. To further evaluate the mighty hemostatic capability of $CS_2/TA_1/SF_1$ hydrogel, it was used for repairing an acute injury with massive hemorrhage that posed a significant fatality risk to traumatic patients in critical situations [45]. To this end, the developed injectable hemostatic hydrogel with robust mechanical strength, rapid blood-triggered shape recovery, high blood uptake capacity, and fast blood absorption speed was utilized in rabbit massive hemorrhage models for evaluating its hemostasis performance further.

First, the rabbit's ear artery was cut off, and blood flow was immediately observed until our prepared material was placed over the wound site (Fig. 5A). As expected, $CS_2/TA_1/SF_1$ hydrogel remained intact and formed a tight adhesion with the lacerated tissue. The binding strength and hemostatic performance of the hydrogel were also evaluated in a harsh condition: rabbit hemorrhagic liver (Fig. 5B & Movie S3, Supplementary data). One wound with a length of 30 mm and a depth of 5 mm was made on the rabbit liver to induce massive bleeding. Due to a strong affinity between hydrogel and tissue surface, a superior procoagulant activity on gushing blood was presented with no doubt. Interestingly, $CS_2/TA_1/SF_1$ hydrogel not only stuck to the wound to prevent the second bleeding but also acted as a resistant barrier to isolate the wounded organ from surrounding tissues to avoid postoperative adhesion [26].

Supplementary video related to this article can be found at https://doi.org/10.1016/j.bioactmat.2021.01.039

We also demonstrated that $CS_2/TA_1/SF_1$ hydrogel could be used to seal cardiac penetration injuries in a rabbit. When the rabbit heart was pierced by a 0.7 mm inner diameter needle, a high-pressure blood expulsion was occurred. As shown in Fig. 5C & Movie S4 (Supplementary data), the bleeding phenomenon was alleviated and stopped entirely after injecting the hydrogel to cover the blood hole. In addition, the hydrogel stuck to the heart tissue tightly, and no second-bleeding was observed later.

Supplementary video related to this article can be found at https://doi.org/10.1016/j.bioactmat.2021.01.039

To further prove the hemostatic efficacy of proposed hydrogel on massive hemorrhage, a lethal femoral artery injury model was created in another rabbit surgical testing. Two hemostatic forceps were used to clamp the artery prior to making a 1.5 mm incision. A significantly reduced blood loss was presented after applying the hydrogel to the incision site, and after 3 min, the bleeding was automatically halted without exerting any external forces. Afterward, the distal end was clipped using surgical scissors, and heavy arterial bleeding recommenced again, indicating the intactness and viability of the femoral artery after treatment with the hydrogel [44]. Because the broken blood vessels were incredibly possible to be blocked by the hydrogel and then caused limb ischemic necrosis of rabbits.

Consequently, we arranged the second hemostasis experiment in the same incision site of repaired blood vessels following the first successful hemostasis to clarify blood fluidity. As shown in Fig. 5D & Movie S5 (Supplementary data), heavy arterial bleeding recommenced again after the distal end was clipped using surgical scissors, indicating intactness and viability of the femoral artery after the hydrogel treatment [42]. Altogether, experiments on these rabbit bleeding models showed that $CS_2/TA_1/SF_1$ hydrogel indeed possessed a high hemostatic efficacy on

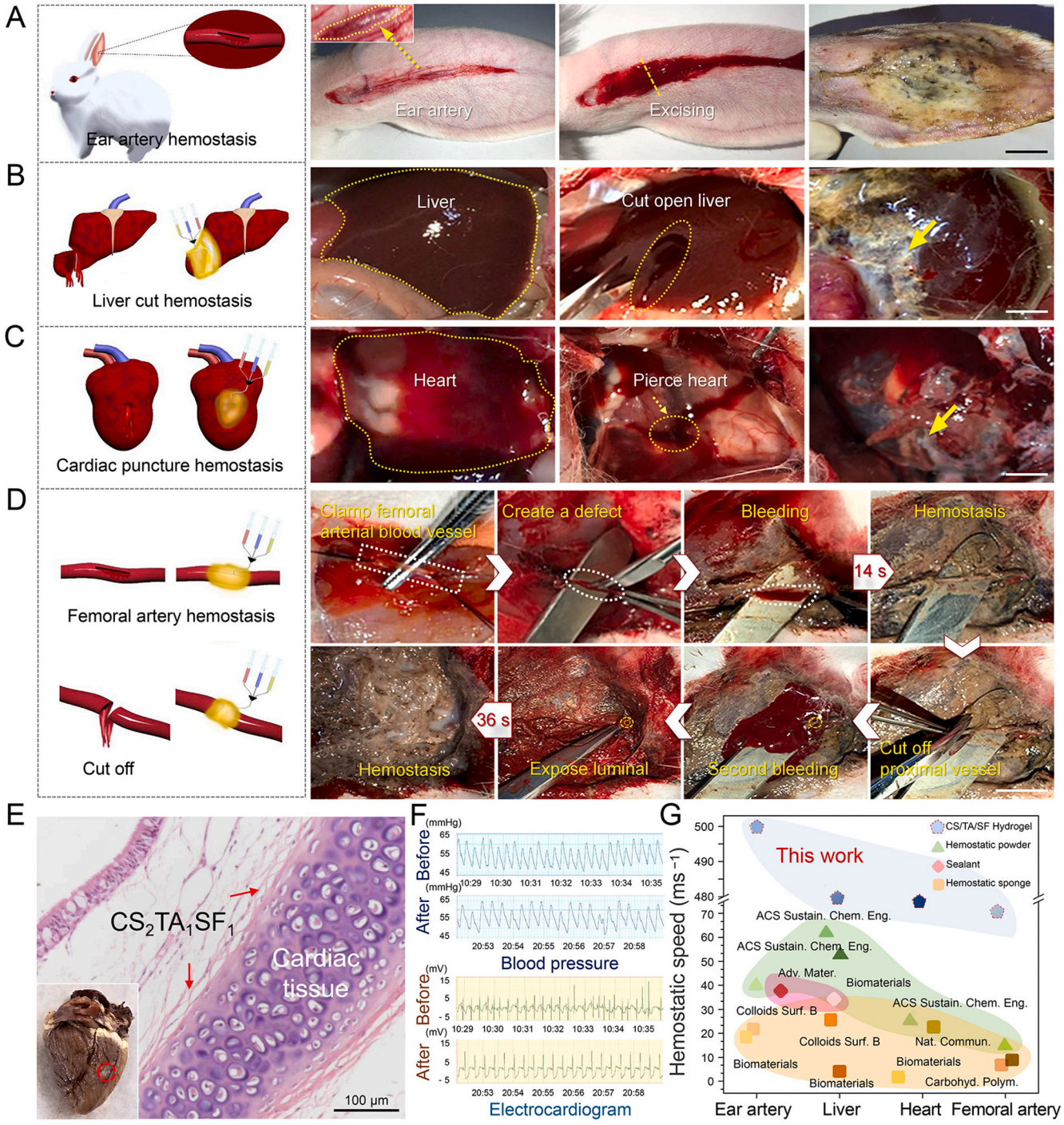

Fig. 5. Hemostatic property and post-operative analysis of $CS_2/TA_1/SF_1$ hydrogel in various massive hemorrhage models of rabbits. (A) Rabbit ear artery, (B) liver, (C) cardiac puncture, and (D) femoral artery injury models treated by hemostatic hydrogel (scale bar = 1 cm). (E) Photograph and H&E staining image of interface reaction between rabbit cardiac tissue and hydrogel. (F) MAP through a rabbit's carotid artery and ECG of a rabbit before and after surgery. (G) Comparison of hemostatic speed between $CS_2/TA_1/SF_1$ hydrogel and previously-reported hemostatic dressings.

massive hemorrhage even under these critical situations. In particular, the adhesion strength of the hydrogel was one of the most important factors for heart and artery hemostasis, where the hydrogel was stably adhered to halt bleeding under arterial blood pressure [46].

Supplementary video related to this article can be found at https://doi.org/10.1016/j.bioactmat.2021.01.039

Rabbits were survived well without any obvious abnormality after a heart operation, and post-operative analysis of cardiac tissues after an autopsy was carried out. The hydrogel still adhered to the defect site without any gap between the hydrogel and heart. No thrombus formed in the vessel, indicating a continuous strong bonding at the healing interface, as observed by tissue section staining (Fig. 5E). In addition, the post-operative degrees of mucosal edema, crusting, and granulation tissue formed in $CS_2/TA_1/SF_1$ hydrogel-applied side were comparable to those of the normal side, and there were almost no inflammatory cells at the interface between the hydrogel and heart tissue, suggesting that our hydrogel achieved an effective and sustained anti-inflammation. Such a superior anti-inflammatory effect could be ascribed to the high biocompatibility and anti-inflammatory activities of TA. Specifically, TA interrupted the propagation stage of lipid autoxidation chain reactions

as effective nitrogen species (RONS) scavengers and played an anti-inflammatory role by affecting phagocytes and blocking inflammatory pathways [47]. The H&E staining results also manifested an excellent bio-safety and availability of the hydrogel.

To access the heart pumping force during preoperative and post-operative, the mean arterial blood pressure (MAP) was continuously recorded in the rabbit after the hydrogel treatment *via* insertion of a 20-gauge catheter into the right carotid artery (Fig. 5F). The animals were alive for the duration of the experiment, and MAP also presented perfect normality. Heart rate and rhythm were also monitored by a continuous electrocardiogram (ECG), and ECG of the rabbit showed no abnormalities during the 72 s nursing period. These results proved that the application of the hydrogel did not affect the basic life activities of organisms. Furthermore, these experimental operations vividly demonstrated the crucial impact of fast wound sealing and strong adhesion on halting blood loss from mobile mammalian organs.

The hemostatic speed of the obtained $CS_2/TA_1/SF_1$ hydrogel was significantly faster than that of other hydrogels previously reported and superior to some commercial organic or inorganic dressings (Fig. 5G) [3,37,40,48–50]. Compared with other hemostatic materials, such unique hydrogel with a dynamic supramolecular-network structure was better at enwinding erythrocytes, and meanwhile, the cationic effect of CS further promoted the blood coagulation. More importantly, the superior wet adhesion ability of the hydrogel sealant definitively formed an enclosure space to improve the hemostatic efficiency further.

4. Conclusions

Timely hemostasis of severe arterial and visceral hemorrhage has been a massive challenge for hemostatic sealant until now. In the current study, an advanced CS/TA/SF hydrogel with a supramolecular cross-linking structure was developed as an efficient hemostatic agent. At first, determining the optimum weight ratios of three primary components based on the orthogonal model was immensely influential, which was examined thoroughly according to the comprehensive performance of the hydrogel. Specifically, $CS_2/TA_1/SF_1$ hydrogel was equipped with optimal hemostatic efficiency, sufficient mechanical properties, and superior absorptive capacity. In the meantime, the strong wet tissue adhesive property of the mussel-inspired hydrogel and intrinsic hemostatic activity of CS led to a synergistic hemostatic performance in acute arterial and cardiac injuries, which was better than other hemostatic materials reported previously. Overall, wound closure ability and hemostasis potential of the hydrogel made it promising in disposing of massive hemorrhages where immediate medical-care was not possible.

CRediT authorship contribution statement

Ziwen Qiao: Conceptualization, Methodology, Writing - original draft. **Xueli Lv:** Conceptualization, Methodology, Writing - original draft. **Shaohua He:** Investigation. **Shumeng Bai:** Validation, Resources, Supervision. **Xiaochen Liu:** Writing - original draft. **Linxi Hou:** Validation, Resources, Supervision. **Jingjing He:** Methodology. **Dongmei Tong:** Methodology. **Renjie Ruan:** Conceptualization, Methodology. **Jin Zhang:** Writing - review & editing, Supervision. **Jianxun Ding:** Resources, Writing - review & editing, Supervision. **Huanghao Yang:** Resources, Writing - review & editing.

Declaration of competing interest

The authors declare that they have no known competing financial interests or personal relationships that could have appeared to influence the work reported in this paper.

Acknowledgments

This work was financially supported by the National Natural Science Foundation of China (Grant No 51903050), the Natural Science Foundation of Fujian Province (Grant No. 2019J01258), the Opening Project of State Key Laboratory of Polymer Materials Engineering (Sichuan University, Grant No. sklpme2019-4-34), the Key Program of Qingyuan Innovation Laboratory (Grant No. 00221002), and the Fuzhou University Testing Fund of Precious Apparatus (Grant No. 2021T025). The authors are grateful to Dr. Di Li from the First Hospital of Jilin University, P. R. China, for the valuable discussion.

Appendix A. Supplementary data

Supplementary data to this article can be found online at https://doi.org/10.1016/j.bioactmat.2021.01.039.

Data availability

All relevant data supporting the findings of this study are either included within the article and its Supplementary Information files or available upon request from the corresponding author.

References

[1] W. Han, B. Zhou, K. Yang, X. Xiong, S. Luan, Y. Wang, Z. Xu, P. Lei, Z. Luo, J. Gao, Y. Zhan, G. Chen, L. Liang, R. Wang, S. Li, H. Xu, Biofilm-inspired adhesive and antibacterial hydrogel with tough tissue integration performance for sealing hemostasis and wound healing, Bioact. Mater. 5 (4) (2020) 768–778.
[2] A.Y. Wang, J. Rafalko, M. MacDonald, X. Ming, R. Kocharian, Absorbable hemostatic aggregates, ACS Biomater. Sci. Eng. 3 (12) (2017) 3675–3686.
[3] E.E. Leonhardt, N. Kang, M.A. Hamad, K.L. Wooley, M. Elsabahy, Absorbable hemostatic hydrogels comprising composites of sacrificial templates and honeycomb-like nanofibrous mats of chitosan, Nat. Commun. 10 (1) (2019) 2307.
[4] F. Arnaud, T. Tomori, W. Carr, A. McKeague, K. Teranishi, K. Prusaczyk, R. McCarron, Exothermic reaction in zeolite hemostatic dressings: QuikClot ACS and ACS+®, Ann. Biomed. Eng. 36 (10) (2008) 1708–1713.
[5] Y. Hong, F. Zhou, Y. Hua, X. Zhang, C. Ni, D. Pan, Y. Zhang, D. Jiang, L. Yang, Q. Lin, Y. Zou, D. Yu, D.E. Arnot, X. Zou, L. Zhu, S. Zhang, H. Ouyang, A strongly adhesive hemostatic hydrogel for the repair of arterial and heart bleeds, Nat. Commun. 10 (1) (2019) 2060.
[6] W. Liu, M. Wang, W. Cheng, W. Niu, M. Chen, M. Luo, C. Xie, T. Leng, L. Zhang, B. Lei, Bioactive antiinflammatory antibacterial hemostatic citrate-based dressing with macrophage polarization regulation for accelerating wound healing and hair follicle neogenesis, Bioact. Mater. 6 (3) (2021) 721–728.
[7] V. Jokinen, E. Kankuri, S. Hoshian, S. Franssila, R.H.A. Ras, Superhydrophobic blood-repellent surfaces, Adv. Mater. 30 (24) (2018) 1705104.
[8] Y. Bu, L. Zhang, G. Sun, F. Sun, J. Liu, F. Yang, P. Tang, D. Wu, Tetra-PEG based hydrogel sealants for *in vivo* visceral hemostasis, Adv. Mater. 31 (28) (2019) 1901580.
[9] L. Wang, X. Zhang, K. Yang, Y.V. Fu, T. Xu, S. Li, D. Zhang, L.N. Wang, C.S. Lee, A novel double-crosslinking-double-network design for injectable hydrogels with enhanced tissue adhesion and antibacterial capability for wound treatment, Adv. Funct. Mater. 30 (1) (2020) 1904156.
[10] X. Zhao, Y. Liang, B. Guo, Z. Yin, D. Zhu, Y. Han, Injectable dry cryogels with excellent blood-sucking expansion and blood clotting to cease hemorrhage for lethal deep-wounds, coagulopathy and tissue regeneration, Chem. Eng. J. 403 (2021) 126329.
[11] W. Chen, R. Wang, T. Xu, X. Ma, Z. Yao, B. Chi, H. Xu, A mussel-inspired poly (γ-glutamic acid) tissue adhesive with high wet strength for wound closure, J. Mater. Chem. B 5 (28) (2017) 5668–5678.
[12] K. Kim, M. Shin, M.-Y. Koh, J.H. Ryu, M.S. Lee, S. Hong, H. Lee, TAPE: A medical adhesive inspired by a ubiquitous compound in plants, Adv. Funct. Mater. 25 (16) (2015) 2402–2410.
[13] S. Bai, X. Zhang, P. Cai, X. Huang, Y. Huang, R. Liu, M. Zhang, J. Song, X. Chen, H. Yang, A silk-based sealant with tough adhesion for instant hemostasis of bleeding tissues, Nanoscale Horiz. 4 (6) (2019) 1333–1341.
[14] H. Yuan, L. Chen, F.F. Hong, A biodegradable antibacterial nanocomposite based on oxidized bacterial nanocellulose for rapid hemostasis and wound healing, ACS Appl. Mater. Interfaces 12 (3) (2020) 3382–3392.
[15] M. Zamani, M. Khafaji, M. Naji, M. Vossoughi, I. Alemzadeh, N. Haghighipour, A biomimetic heparinized composite silk-based vascular scaffold with sustained antithrombogenicity, Sci. Rep. 7 (1) (2017) 4455.
[16] Y. Fang, Y. Xu, Z. Wang, W. Zhou, L. Yan, X. Fan, H. Liu, 3D porous chitin sponge with high absorbency, rapid shape recovery, and excellent antibacterial activities for noncompressible wound, Chem. Eng. J. 388 (2020) 124169.
[17] S. Bai, S. Liu, C. Zhang, W. Xu, Q. Lu, H. Han, D.L. Kaplan, H. Zhu, Controllable transition of silk fibroin nanostructures: An insight into *in vitro* silk self-assembly process, Acta Biomater. 9 (8) (2013) 7806–7813.
[18] R. Wang, J. Li, W. Chen, T. Xu, S. Yun, Z. Xu, Z. Xu, T. Sato, B. Chi, H. Xu, A biomimetic mussel-inspired ε-poly-L-lysine hydrogel with robust tissue-anchor and anti-infection capacity, Adv. Funct. Mater. 27 (8) (2017) 1604894.

[19] O.V. Kim, R.I. Litvinov, M.S. Alber, J.W. Weisel, Quantitative structural mechanobiology of platelet-driven blood clot contraction, Nat. Commun. 8 (1) (2017) 1274.
[20] A.R. Scott, Polymers: Secrets from the deep sea, Nature 519 (7544) (2015) S12–S13.
[21] J.J. Wilker, Positive charges and underwater adhesion, Science 349 (6248) (2015) 582–583.
[22] X. Zhao, B. Guo, H. Wu, Y. Liang, P.X. Ma, Injectable antibacterial conductive nanocomposite cryogels with rapid shape recovery for noncompressible hemorrhage and wound healing, Nat. Commun. 9 (1) (2018) 2784.
[23] C. Wang, W. Luo, P. Li, S. Li, Z. Yang, Z. Hu, Y. Liu, N. Ao, Preparation and evaluation of chitosan/alginate porous microspheres/*Bletilla striata* polysaccharide composite hemostatic sponges, Carbohydr. Polym. 174 (2017) 432–442.
[24] X. Fan, M. Li, Q. Yang, G. Wan, Y. Li, N. Li, K. Tang, Morphology-controllable cellulose/chitosan sponge for deep wound hemostasis with surfactant and pore-foaming agent, Mater. Sci. Eng. C Mater. Biol. Appl. 118 (2021) 111408.
[25] A. Shukla, J.C. Fang, S. Puranam, F.R. Jensen, P.T. Hammond, Hemostatic multilayer coatings, Adv. Mater. 24 (4) (2012) 492–496.
[26] X. Zhao, Y. Liang, Y. Huang, J. He, Y. Han, B. Guo, Physical double-network hydrogel adhesives with rapid shape adaptability, fast self-healing, antioxidant and NIR/pH stimulus-responsiveness for multidrug-resistant bacterial infection and removable wound dressing, Adv. Funct. Mater. 30 (17) (2020) 1910748.
[27] W. Zhang, X. Ma, Y. Li, D. Fan, Preparation of smooth and macroporous hydrogel *via* hand-held blender for wound healing applications: *In vitro* and *in vivo* evaluations, Biomed. Mater. 15 (5) (2020), 055032.
[28] Y. Si, L.H. Wang, X.Q. Wang, N. Tang, J.Y. Yu, B. Ding, Ultrahigh-water-content, superelastic, and shape-memory nanofiber-assembled hydrogels exhibiting pressure-responsive conductivity, Adv. Mater. 29 (24) (2017) 1700339.
[29] A. Gupta, M. Kowalczuk, W. Heaselgrave, S.T. Britland, C. Martin, I. Radecka, The production and application of hydrogels for wound management: A review, Eur. Polym. J. 111 (2019) 134–151.
[30] J. Iglesias, E. García de Saldaña, J.A. Jaén, On the tannic acid interaction with metallic iron, Hyperfine Interact. 134 (1) (2001) 109–114.
[31] B. Li, L. Wang, F. Xu, X. Gang, U. Demirci, D. Wei, Y. Li, Y. Feng, D. Jia, Y. Zhou, Hydrosoluble, UV-crosslinkable and injectable chitosan for patterned cell-laden microgel and rapid transdermal curing hydrogel *in vivo*, Acta Biomater. 22 (2015) 59–69.
[32] J.P. Quiñones, C. Roschger, A. Zierer, C. Peniche, O. Brüggemann, Steroid-grafted silk fibroin conjugates for drug and agrochemical delivery, Eur. Polym. J. 119 (2019) 169–175.
[33] R. Liu, J. Zhu, J. Luo, X. Liu, Synthesis and application of novel UV-curable hyperbranched methacrylates from renewable natural tannic acid, Prog. Org. Coat. 77 (1) (2014) 30–37.
[34] M. Shin, J.H. Ryu, J.P. Park, K. Kim, J.W. Yang, H. Lee, DNA/tannic acid hybrid gel exhibiting biodegradability, extensibility, tissue adhesiveness, and hemostatic ability, Adv. Funct. Mater. 25 (8) (2015) 1270–1278.
[35] H. Fan, L. Wang, X. Feng, Y. Bu, D. Wu, Z. Jin, Supramolecular hydrogel formation based on tannic acid, Macromolecules 50 (2) (2017) 666–676.
[36] J. Shin, J.S. Lee, C. Lee, H.J. Park, K. Yang, Y. Jin, J.H. Ryu, K.S. Hong, S.H. Moon, H.M. Chung, H.S. Yang, S.H. Um, J.W. Oh, D.I. Kim, H. Lee, S.W. Cho, Tissue adhesive catechol-modified hyaluronic acid hydrogel for effective, minimally invasive cell therapy, Adv. Funct. Mater. 25 (25) (2015) 3814–3824.
[37] G. Lan, B. Lu, T. Wang, L. Wang, J. Chen, K. Yu, J. Liu, F. Dai, D. Wu, Chitosan/gelatin composite sponge is an absorbable surgical hemostatic agent, Colloids Surf. B Biointerfaces 136 (2015) 1026–1034.
[38] Y. Yu, P. Li, C. Zhu, N. Ning, S. Zhang, G.J. Vancso, Multifunctional and recyclable photothermally responsive cryogels as efficient platforms for wound healing, Adv. Funct. Mater. 29 (35) (2019) 1904402.
[39] R.W. Farndale, J.J. Sixma, M.J. Barnes, P.G. De Groot, The role of collagen in thrombosis and hemostasis, J. Thromb. Haemost. 2 (4) (2004) 561–573.
[40] X. Zhao, H. Wu, B. Guo, R. Dong, Y. Qiu, P.X. Ma, Antibacterial anti-oxidant electroactive injectable hydrogel as self-healing wound dressing with hemostasis and adhesiveness for cutaneous wound healing, Biomaterials 122 (2017) 34–47.
[41] N. Annabi, Y.N. Zhang, A. Assmann, E.S. Sani, G. Cheng, A.D. Lassaletta, A. Vegh, B. Dehghani, G.U. Ruiz-Esparza, X. Wang, S. Gangadharan, A.S. Weiss, A. Khademhosseini, Engineering a highly elastic human protein–based sealant for surgical applications, Sci. Transl. Med. 9 (410) (2017) eaai7466.
[42] M.V. Lomova, A.I. Brichkina, M.V. Kiryukhin, E.N. Vasina, A.M. Pavlov, D. A. Gorin, G.B. Sukhorukov, M.N. Antipina, Multilayer capsules of bovine serum albumin and tannic acid for controlled release by enzymatic degradation, ACS Appl. Mater. Interfaces 7 (22) (2015) 11732–11740.
[43] G. Bao, S. Suresh, Cell and molecular mechanics of biological materials, Nat. Mater. 2 (11) (2003) 715–725.
[44] L.I.F. Moura, A.M.A. Dias, E. Carvalho, H.C. de Sousa, Recent advances on the development of wound dressings for diabetic foot ulcer treatment—a review, Acta Biomater. 9 (7) (2013) 7093–7114.
[45] N. Mackman, R.E. Tilley, N.S. Key, Role of the extrinsic pathway of blood coagulation in hemostasis and thrombosis, Arterioscler. Thromb. Vasc. Biol. 27 (8) (2007) 1687–1693.
[46] P. Sahariah, M. Másson, Antimicrobial chitosan and chitosan derivatives: A review of the structure–activity relationship, Biomacromolecules 18 (11) (2017) 3846–3868.
[47] Z. Wei, L. Wang, C. Tang, S. Chen, Z. Wang, Y. Wang, J. Bao, Y. Xie, W. Zhao, B. Su, C. Zhao, Metal-phenolic networks nanoplatform to mimic antioxidant defense system for broad-spectrum radical eliminating and endotoxemia treatment, Adv. Funct. Mater. 30 (49) (2020) 2002234.
[48] M. Helmes, K. Trombitás, T. Centner, M. Kellermayer, S. Labeit, W.A. Linke, H. Granzier, Mechanically driven contour-length adjustment in rat cardiac titin's unique N2B sequence, Circ. Res. 84 (11) (1999) 1339–1352.
[49] N.D. Sanandiya, S. Lee, S. Rho, H. Lee, I.S. Kim, D.S. Hwang, Tunichrome-inspired pyrogallol functionalized chitosan for tissue adhesion and hemostasis, Carbohydr. Polym. 208 (2019) 77–85.
[50] C. Feng, J. Li, G.S. Wu, Y.Z. Mu, M. Kong, C.Q. Jiang, X.J. Cheng, Y. Liu, X.G. Chen, Chitosan-coated diatom silica as hemostatic agent for hemorrhage control, ACS Appl. Mater. Interfaces 8 (50) (2016) 34234–34243.